PCCP

PAPER

View Article Online
View Journal | View Issue

Cite this: *Phys. Chem. Chem. Phys.*, 2014, **16**, 26193

Rational design of tetraphenylethylene-based luminescent down-shifting molecules: photophysical studies and photovoltaic applications in a CdTe solar cell from small to large units†

Yilin Li,[ab] Zhipeng Li,[a] Tursunjan Ablekim,[c] Tianhui Ren*[a] and Wen-Ji Dong*[b]

Received 7th August 2014,
Accepted 17th October 2014

DOI: 10.1039/c4cp03521f

www.rsc.org/pccp

A rational design strategy of novel fluorophores for luminescent down-shifting (LDS) application was proposed and tested in this paper. Three new fluorophores (**1a–c**) with specific intramolecular charge transfer (ICT) and aggregation-induced emission (AIE) characteristics were synthesized as LDS molecules for increasing the output short circuit current density (J_{sc}) of a CdTe solar cell. Photophysical studies of their solution and solid states, and photovoltaic measurements of their PMMA solid films applied on a CdTe solar cell suggested that the specific spectroscopic properties and J_{sc} enhancement effects of these molecules were highly related to their chemical structures. The J_{sc} enhancement effects of these fluorophores were measured on both a CdTe small cell and a large panel. An increase in the output J_{sc} by as high as 5.69% for a small cell and 8.88% for a large panel was observed. Compared to a traditional LDS molecule, Y083, these fluorophores exhibited more superior capabilities of LDS.

Introduction

The cadmium telluride (CdTe) solar cell has been considered to be one of the most promising photovoltaic (PV) technologies in recent years and accounts for a significant portion of the PV market in the future because of its low-cost and easy-manufacture, compared to the traditional crystalline silicon (c-Si) solar cell.[1,2] However, the CdTe solar cell exhibits a poor spectral response to the short-wavelength region (<500 nm) due to the absorption of the n-type cadmium sulfide (CdS, E_g = 2.42 eV) 'window' layer in the cell structure, which inevitably leads to some degree of output current loss.[3,4] To eliminate or minimize this issue, numerous efforts have been made to optimize the cell structure to reduce the absorption effect of the CdS layer.[5–7] However, the most effective and efficient approach is to use a luminescent down-shifting (LDS) layer that is placed on the front surface of the cell to modify the spectrum of the incident light.[8,9] A LDS layer is typically a polymer sheet with luminescent molecules (fluorophores) embedded in it, which can convert the short-wavelength photons into long-wavelength photons by the process of photon absorption and emission.

Until now, BASF Lumogen F dye Yellow 083 (Y083) has been the most widely used fluorophore in research for the LDS application to improve the output short circuit current density (J_{sc}) of the CdTe solar cell.[10–12] Early studies showed that applying a LDS film of Y083 on the front surface of a CdTe solar cell could enhance its output J_{sc} by as high as 33% through conversion of photons from a wavelength below 500 nm to over 500 nm.[9] However, as the cell fabrication with new technologies is improved, the poor short-wavelength response of the cell is gradually solved at the cell structure level. Compared to an old type CdTe solar cell, the new one exhibits a nearly doubled short-wavelength spectral response. Consequently, the J_{sc} enhancement effect (ΔJ_{sc}%) of Y083 on the new type of CdTe solar cell decreases to 4%.[13] Such a significant decrease in the ΔJ_{sc}% value is attributed to two aspects – an increase of the parasitic absorption effect and an insufficient emission spectral match. The increased parasitic absorption effect of Y083 is the result of significantly increased spectral overlap between absorption of Y083 and the spectral response of the new type of CdTe solar cell in the wavelength

[a] *School of Chemistry and Chemical Engineering, Shanghai Jiao Tong University, Shanghai 200240, China. E-mail: thren@sjtu.edu.cn*
[b] *School of Chemical Engineering and Bioengineering, Washington State University, Pullman, WA 99164, USA. E-mail: wdong@vetmed.wsu.edu*
[c] *Center for Materials Research, Washington State University, Pullman, WA 99164, USA*

† Electronic supplementary information (ESI) available: Synthesis and characterization of compounds **2–6**, some experimental details and schematic structures of devices with LDS films on the front surfaces of solar cell devices. See DOI: 10.1039/c4cp03521f

region of 400–500 nm. Such an increased parasitic absorption effect gives rise to the J_{sc} loss (J_{loss}%) of 6.6%, compared to 3.8% for the old type cell (Fig. S1, ESI†). The insufficient emission spectral match originated from the mismatch between the emission spectrum of Y083 and the maximum spectral response (600–800 nm) of the CdTe solar cell. The emission spectral matching factor (F_{em}) is 0.70 for the old type CdTe solar cell and 0.84 for the new one (Fig. S2, ESI†). Besides the high J_{loss}% and low F_{em}, application of Y083 as a LDS material also suffers from its fluorescence self-quenching in the solid state because of its perylene-based planar molecule, possessing the potential for π–π stacking. The fluorescence self-quenching enables Y083 to have a quantum yield of 0.92 compared to its near unity value (0.99) in solution,[11,14] which results in about 7% loss in photon conversion efficiency during the LDS process.

To avoid these problems and improve its application in LDS, a fluorophore should have a more blue-shifted absorption and a more red-shifted emission than that of Y083, *i.e.* have a large Stokes shift. In addition, a minimized potential π–π stacking effect and an optimized fluorescence quantum yield in the solid state are also desired. To increase the Stokes shift of a fluorophore, one approach is to construct a molecular system structured with donor (D) and acceptor (A) moieties to achieve an intramolecular charge transfer (ICT).[15,16] For such a D–A type fluorophore, its absorption spectrum is dominated by the photophysical properties of the donor while its emission is related to the charge transfer (CT) rate from the donor to the acceptor upon molecular excitation. A high CT rate will result in a large change in the transition dipole moment of the molecule, and consequently induces a large Stokes shift.[17] Our previous studies have shown that the absorption and emission spectra as well as the Stokes shift can be fine-tuned by manipulating the charge densities of the donor and/or the acceptor to achieve various CT rates.[18,19] On the other hand, the π–π stacking effect associated with Y083 can be minimized or prevented if the molecular structure is more flexible.[20,21] Recent studies show that fluorophores with tetraphenylethylene (TPE) structures exhibit aggregation-induced emission (AIE) characteristics that can help prevent the π–π stacking effect and thus increase the solid state fluorescence quantum yield.[22,23] The mechanism of AIE is probably due to the molecular restricted internal rotation (RIR) of the free-rotated phenyl rings that impedes the non-radiative decay pathway during the emission process.[24]

Therefore, to overcome the disadvantages of Y083, we propose a rational design strategy to take advantage of both molecular ICT and AIE mechanisms in designing more effective and efficient LDS molecules. In this paper, we report three newly-designed fluorophores (**1a–c**) with specific ICT and AIE characteristics. Their photophysical properties as well as their J_{sc} enhancement effects as LDS molecules are highly related to their chemical structures. Compared to Y083, all synthesized fluorophores exhibit large Stokes shifts (up to 170 nm) with a blue-shifted absorption and a red-shifted emission as well as high solid state fluorescence quantum yields (up to 0.99). Thereby, they have a less parasitic absorption effect (J_{loss}% as low as 4.0%) and/or higher degree of emission spectral matching (F_{em} up to 0.86) with the CdTe solar cell than that of Y083 (6.2% and 0.81, respectively) for the CdTe solar cell used in our experiment. Their J_{sc} enhancement effects were measured on both a small CdTe solar cell and a large CdTe solar panel. Applying their solid PMMA films on a small CdTe solar cell and a large CdTe solar panel enhances the output J_{sc} by as high as 5.69% and 8.88%, respectively.

Results and discussion

Molecular synthesis

The molecular structures of fluorophores **1a–c** and their synthetic routes are demonstrated in Scheme 1. All synthesized fluorophores contain the structures of tetraphenylethylene (TPE) and a di-cyano (DCN) group. The major synthetic techniques are the Pd-catalyzed Suzuki coupling to form the TPE group and the Knoevenagel condensation to form the DCN group. In addition to the synthesis of fluorophores **1a–c** shown

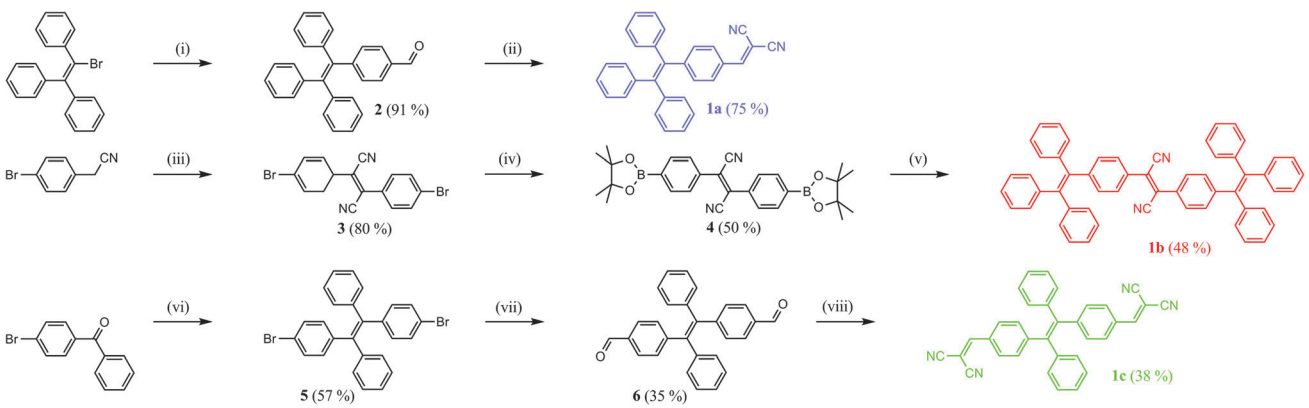

Scheme 1 Synthetic routes and molecular structures of fluorophores **1a–c**. Reaction reagents and conditions: (i) 4-formylphenylboronic acid, $Pd(dppf)Cl_2$, K_2CO_3, MeOH, and toluene, 75 °C, 16 h; (ii) malononitrile, Al_2O_3 (basic), DCM, reflux, 16 h; (iii) I_2, Et_2O, −78 °C, CH_3ONa, MeOH, −78 °C, 30 min; (iv) B_2pin_2, $Pd(dppf)Cl_2$, KOAc, 1,4-dioxane, 100 °C, 16 h; (v) 2-bromo-1,1,2-triphenylethylene, $Pd(PPh_3)_4$, K_2CO_3 (aq), MeOH, toluene, 80 °C, 16 h; (vi) $TiCl_4$, Zn dust, THF, reflux, 20 h; (vii) DMF, *n*-BuLi, −78 °C, 16 h; and (viii) malononitrile, Al_2O_3 (basic), DCM, reflux, 16 h.

in the Experimental section, the detailed synthetic procedures and characterization of other compounds are described in the ESI.† Since our molecular design strategy is to use the TPE group as a charge donor (D) and the DCN group as a charge acceptor (A), fluorophores **1a–c** can be considered as D–A, D–A–D and A–D–A type fluorophores, respectively.

After synthesis, the thermal stabilities of these fluorophores were investigated by TGA and DSC (Fig. S3, ESI†). The decomposition temperature (T_d) of fluorophores **1a–c** is 263 °C, 365 °C and 308 °C, respectively. The melting temperature (T_m) of fluorophores **1a** and **1b** is 156 °C and 270 °C, respectively. Fluorophore **1c** did not show apparently melting down during the measurement. The results of the thermal stabilities of these synthesized fluorophores suggest that they are highly thermally stable and worth for further photophysical studies and photovoltaic applications.

Photophysical studies

The photophysical properties of fluorophores **1a–c** were studied in both solution and solid states. Solution samples were prepared by dissolving each fluorophore in 1,4-dioxane. Solid samples were prepared by doping each fluorophore in PMMA to form solid films. Fig. 1a depicts their absorption and emission spectra in 1,4-dioxane solution while Fig. 1b depicts their absorption and emission spectra in solid PMMA film. For comparison, absorption and emission spectra of Y083, the spectral response of a CdTe solar cell and an AM1.5G solar spectrum (photon distribution) are also shown in Fig. 1b. The pertinent photophysical parameters are summarized in Table 1.

It is noted in Table 1 that there is not much difference in the maximum absorption wavelength (λ_{abs}) of fluorophores **1a–c** between their 1,4-dioxane solution samples and PMMA solid samples. This can be explained by the Franck–Condon principle that the absorption process is environmentally insensitive because the transition speed of the electron is very fast in femtoseconds than that of the molecular structure relaxation.[26] A slight difference is found in their maximum emission wavelength (λ_{em}) because the emission process is more environmentally dependent. It is well-known that 1,4-dioxane has low solvent polarity. Therefore, the large Stokes shift (147–167 nm) of these fluorophores is believed not coming from the solvent effect of 1,4-dioxane but the intramolecular charge transfer (ICT) process that is intrinsically associated with fluorophores **1a–c**. Such an ICT process also leads to large Stokes shifts (139–170 nm) of these fluorophores in the solid state, which are much larger than Y083 (64 nm). Besides the difference in the Stokes shift, large differences in the molar absorption coefficient (ε) and fluorescence quantum yield (Φ_f) are also found among these fluorophores. The low ε value in the solid state suggests that these fluorophores exhibit a low photon absorption probability due to the fixed molecular conformation, compared to the free-rotating molecular conformation in solution. The lower Φ_f value in solution than that in the solid is known to be due to the AIE phenomenon that TPE-based AIE fluorophores usually exhibit extreme low fluorescence quantum yields in solution but high fluorescence quantum yields in the solid. Compared to Y083, except for fluorophore **1c** (0.81) other two fluorophores exhibit higher quantum yields (0.99 for **1a** and 0.98 for **1b**) than that of

Table 1 Absorption wavelength (λ_{abs}), emission wavelength (λ_{em}), Stokes shift ($\Delta\lambda = \lambda_{em} - \lambda_{abs}$), molar absorption coefficient (ε) and fluorescence quantum yield (Φ_f) of each fluorophore in both 1,4-dioxane solution and the solid PMMA film

	Solution			Solid			
Parameters	**1a**	**1b**	**1c**	**1a**	**1b**	**1c**	Y083
λ_{abs} (nm)	389	407	392	392	406	397	476
λ_{em} (nm)	536	574	546	532	576	533	540
$\Delta\lambda$ (nm)	147	167	154	140	170	139	64
ε (M^{-1} cm^{-1})	27 454	32 210	28 419	10 347	11 824	10 941	19 785
Φ_f[a]	0.0023	0.048	0.0046	0.99	0.98	0.81	0.92

[a] Φ_f of solution samples were measured using 4-dimethylamino-4′-nitrostilbene (Φ_f = 0.53 in benzene) as standard; Φ_f of solid samples (including Y083) were measured using an integrating sphere.[25]

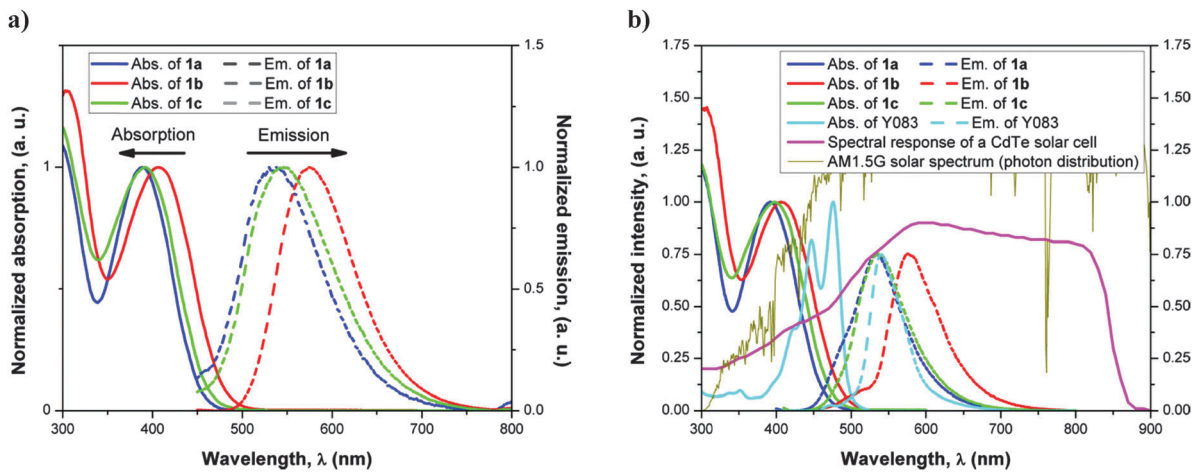

Fig. 1 Absorption and emission spectra of fluorophores **1a–c** in (a) 1,4-dioxane solution and (b) the solid PMMA film. In (b), the absorption and emission spectra of Y083, the spectral response of a CdTe solar cell and an AM1.5G solar spectrum (photon distribution) are also illustrated for comparison.

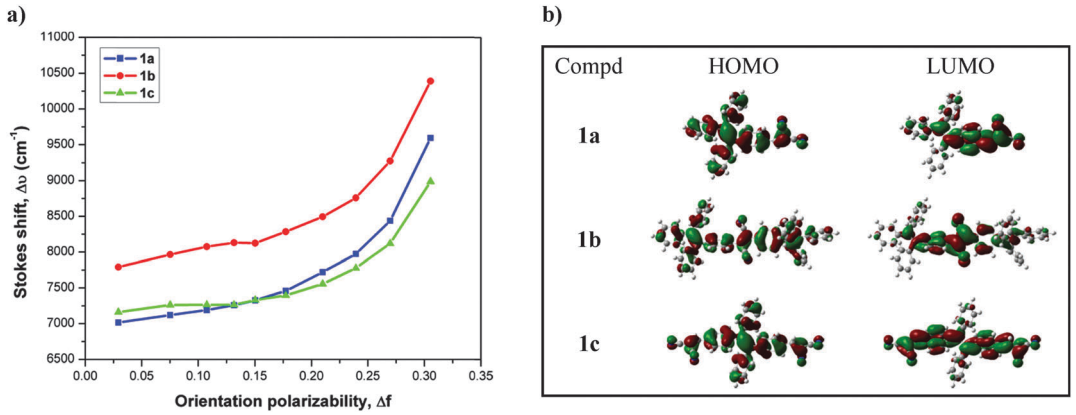

Fig. 2 (a) Relationship between solvent orientation polarizability (Δf) and Stokes shift (in wavenumber) and (b) charge distribution on the HOMO and LUMO of fluorophores **1a–c**.

Y083 (0.92). It is believed that their large Stokes shifts and high quantum yields are due to their intrinsic ICT and AIE characteristics, which will be further studied.

We believe that the large Stokes shifts associated with these fluorophores are due to the ICT process that occurred within the fluorophores upon excitation. Their ICT characteristics were investigated by solvatochromism measurements and theoretical calculations. In the solvatochromism measurements, each fluorophore was dissolved in 1,4-dioxane–acetonitrile mixtures and the absorption and emission wavelengths were measured to obtain the Stokes shifts. The Stokes shifts (in wavenumber) are plotted *vs.* solvent orientation polarizability (Δf) – a parameter described in the Lippert–Mataga equation ($\Delta f = (J-1)/(2J+1) - (n^2-1)/(2n^2+1)$, where J is the dielectric constant and n is the refractive index),[27–29] – in Fig. 2a. The theoretical calculations were performed using DFT and TD-DFT methods at the B3LYP/6-31G(d) level. The molecular charge distribution on the HOMO and LUMO of each fluorophore is depicted in Fig. 2b. The maximum Stokes shift change upon Δf ($\Delta(\Delta\upsilon)/\Delta(\Delta f)$), transition dipole moment change ($|\mu_e - \mu_g|$) and the calculated charge transfer (CT) rate are listed in Table 2. The detailed experimental and theoretical procedures and methods are described in the ESI.†

It is noted that all the synthesized fluorophores exhibit ICT characteristics suggested by changing their Stokes shifts non-linearly with the increase of Δf in solvatochromism measurements (Fig. 2a), and the charge transfer processes were observed from the ground state to the excited state based on the charge distribution of the HOMO and LUMO in theoretical calculations (Fig. 2b). In Table 2, fluorophore **1b** exhibits the highest $\Delta(\Delta\upsilon)/\Delta(\Delta f)$ value (9418 cm^{-1}), indicating that it possesses the strongest ICT characteristic among all fluorophores. Such strong ICT characteristic of fluorophore **1b** comes from the huge transition dipole moment change (27.5 D) from the ground state to the excited state associated with a high CT rate that 57% charge flows forward from the TPE group to the DCN group upon molecular absorption and 54% flows backward upon molecular emission. For fluorophore **1c**, its $\Delta(\Delta\upsilon)/\Delta(\Delta f)$ value (3984 cm^{-1}) is the lowest with a relatively small change in its transition dipole moment (12.6 D). Its CT rate is only 39% during the absorption and 27% during the emission. Furthermore, it is worth noting that the ICT characteristics of these fluorophores are closely related to their molecular structures. Compared to fluorophore **1a**, fluorophore **1b** has one more TPE group (charge donor) in its structure while fluorophore **1c** has one more DCN group (charge acceptor). Fluorophore **1b** exhibits the strongest ICT characteristic while fluorophore **1c** exhibits the weakest. The order of transition dipole moment change in solvatochromism measurements and the calculated CT rate in theoretical calculations of fluorophores **1a–c** is **1b** > **1a** > **1c**. Therefore, the strength of ICT characteristic of fluorophores **1a–c** is **1b** > **1a** > **1c**.

Table 2 Maximum Stokes shift change upon Δf ($\Delta(\Delta\upsilon)/\Delta(\Delta f)$), transition dipole moment change ($|\mu_e - \mu_g|$) and the calculated charge transfer (CT) rate of fluorophores **1a–c**

	Solvatochromism		CT rate[c]	
Compd	$\Delta(\Delta\upsilon)/\Delta(\Delta f)$[a] ($cm^{-1}$)	$\lvert\mu_e - \mu_g\rvert$ (D)[b]	Absorption (Gd → Ex) (%)	Emission (Ex → Gd) (%)
1a	9343	13.6 ± 1.3	51	51
1b	9418	27.5 ± 2.6	57	54
1c	3984	12.6 ± 1.2	39	27

[a] $\Delta(\Delta\upsilon)/\Delta(\Delta f) = (\Delta\upsilon_{max} - \Delta\upsilon_{min})/(\Delta f_{max} - \Delta f_{min})$. [b] Calculated from the linear fitting results of the Lipper–Mataga equation. [c] Calculated from the difference in charge distribution on donor (TPE group) between the ground (Gd) and excited (Ex) states.

It is noted in Table 1 that fluorophores **1a–c** exhibit a huge increase in the fluorescence quantum yield (Φ_f) from their 1,4-dioxane solution to the solid PMMA film. Such an increase in Φ_f can be attributed to the aggregation-induced emission (AIE) characteristics of these fluorophores. The AIE characteristics of these fluorophores were investigated by measuring Φ_f and the fluorescence lifetime (τ_f). Φ_f values were measured in acetonitrile–water mixtures from 40% to 95% water fraction. τ_f values were measured in 95% water fraction of the acetonitrile–water mixture (fitted by a two-exponential decay equation) and solid PMMA films (fitted by a single-exponential decay equation, the fitting methods are described in the ESI†).

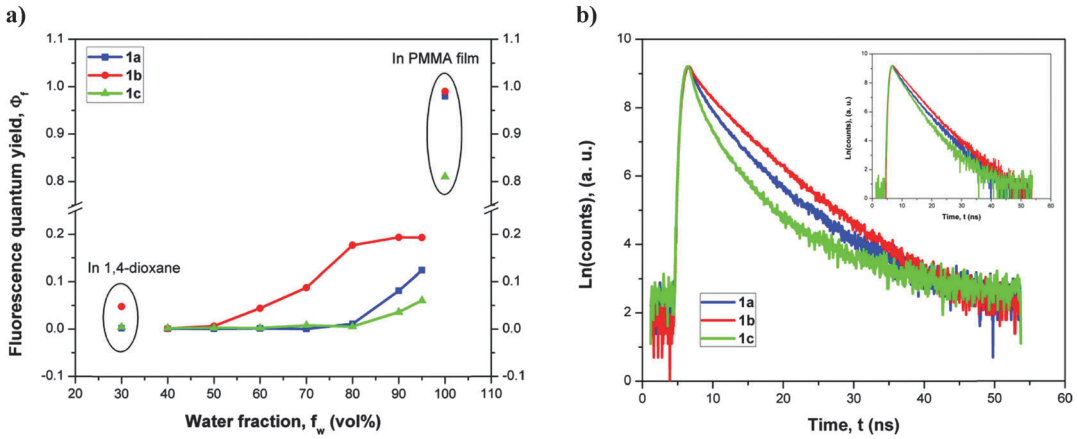

Fig. 3 (a) Fluorescence quantum yields (Φ_f) in acetonitrile–water mixtures (fluorophore concentration is 15 μM; Φ_f values were measured using 4-dimethylamino-4′-nitrostilbene (Φ_f = 0.53 in benzene) as standard and the values in 1,4-dioxane and PMMA film are also depicted for comparison); and (b) the fluorescence lifetime (τ_f) in 95% water fraction of the acetonitrile–water mixture and solid PMMA films (inset) of fluorophores **1a–c**.

The experimental results are shown in Fig. 3 and the fluorescence lifetime parameters are listed in Table 3.

Because all fluorophores are structurally hydrophobic, they are expected to precipitate out as nanoparticles (aggregation phenomenon) in high water content solutions. And such an aggregation will lead to the increase in fluorescence quantum yields (Φ_f) of these fluorophores if they possess AIE characteristics. A significant increase was found in fluorescence intensity measurements of fluorophores **1a–c** in 40% and 90% mixtures (Fig. S4, ESI†). In Fig. 3a, with the increase in the water fraction in the mixture, the Φ_f values of fluorophores **1a–c** began to increase at the point at 70%, 50% and 80%, indicating that all fluorophores exhibit AIE characteristics and fluorophore **1b** has the highest degree of aggregation while fluorophore **1c** has the lowest. The AIE characteristic is from the molecular restricted internal rotation (RIR) of the TPE group in the fluorophore in the solid, which impedes the non-radiative decay pathway and thus boosts the fluorescence quantum yield. The AIE mechanism was further investigated by measuring the fluorescence lifetimes of fluorophores **1a–c** in the solvent mixture and solid state. In Fig. 3b, it is noted that the fluorophores **1a–c** exhibited a two-exponential decay pattern in 95% water fraction solution while a single-exponential decay pattern in the solid PMMA film. This is because there were two components in 95% water fraction solution – free molecules in solution and the aggregated molecules in the solid form. As shown in Table 3, the shorter lifetimes (1.00–1.37 ns) can be ascribed to the molecules in solution while the longer ones (3.89–4.67 ns) to those in solid, which are consistent with the lifetimes (2.95–3.32 ns) directly measured from the solid PMMA films. From the point of view of the molecular structure of each fluorophore, fluorophore **1b** exhibits the highest fluorescence quantum yield with the longest lifetime in its solid state due to one more TPE group in its structure while fluorophore **1c** exhibits the lowest fluorescence quantum yield and the shortest lifetime due to one more DCN group. Therefore, the strength of AIE characteristics of fluorophores **1a–c** is **1b** > **1a** > **1c**.

Table 3 Individual lifetime (τ_1 and τ_2) and average lifetime ($\langle\tau\rangle$ or τ) in the solvent mixture (f_w = 95%) and the solid PMMA film

	Solvent mixture (f_w = 95%)				Solid PMMA film	
Compounds	τ_1 (ns)	τ_2 (ns)	$\langle\tau\rangle$ (ns)	r^2	τ (ns)	r^2
1a	1.37	4.67	3.78	0.9995	3.32	0.9984
1b	1.71	5.47	4.85	0.9995	3.99	0.9990
1c	1.00	3.89	2.71	0.9987	2.95	0.9987

Photovoltaic application

From Fig. 1b, it is noted that the absorption spectra of fluorophores **1a–c** cover the weak spectral response region of the CdTe solar cell while their emission spectra are under the strong spectral response region of the cell. Therefore, it is worth investigating the luminescent down-shifting (LDS) effect of these fluorophores on the short circuit current density (J_{sc}) of the CdTe solar cell. To evaluate the J_{sc} enhancement effects of these synthesized fluorophores, LDS films containing each of the synthesized fluorophores as well as Y083 with the weight concentration from 0.2 to 2.0% were prepared. The detailed preparation method is described in the Experimental section. The spectral response (EQE) of the CdTe solar cell used in the measurement is depicted in Fig. 1b, which is similar to that of the large CdTe module depicted in Fig. S1b (ESI†). Three different methods were used in the LDS measurements to evaluate the J_{sc} enhancement abilities of the LDS films. The first method is to directly measure the photocurrent (I_{ph}) using a multimeter under the incident light from a solar simulator. The second method is to measure the *I–V* curve using a sourcemeter to obtain the short circuit current (I_{sc}) under the same incident light as the first method. The third method is to measure the cell EQE and the results were integrated with the AM1.5G solar spectrum to afford the J_{sc} value. The J_{sc} enhancement values (ΔJ_{sc}%), calculated from the three methods are denoted $\Delta J_{sc}\%_{ph}$ (= $I_{ph}/I_{ph,0} - 1$), $\Delta J_{sc}\%_{I-V}$ (= $I_{sc}/I_{sc,0} - 1$) and $\Delta J_{sc}\%_{EQE}$ (= $J_{sc}/J_{sc,0} - 1$), respectively, where the subscript '0' stands for the bare cell without the LDS layer. The ΔJ_{sc}% values

Table 4 $\Delta J_{sc}\%$ obtained from each method and its average value of a 2.0% LDS film of fluorophores **1a–c** as well as Y083 ($J_{loss}\%$, F_{em} and $\Phi_{f,solid}$ are also listed for comparison)

Compd	$\Delta J_{sc}\%_{ph}$ (%)	$\Delta J_{sc}\%_{I-V}$ (%)	$\Delta J_{sc}\%_{EQE}$ (%)	$\Delta J_{sc}\%_{avg}$ (%)	$J_{loss}\%^{a}$ (%)	$F_{em}{}^{a}$	$\Phi_{f,solid}{}^{b}$
1a	4.12	3.93	3.80	3.95 ± 0.16	4.0	0.76	0.99
1b	5.94	6.04	5.10	5.69 ± 0.52	6.1	0.86	0.98
1c	1.61	1.81	1.79	1.74 ± 0.11	4.9	0.78	0.81
Y083	3.48	3.51	2.85	3.28 ± 0.37	6.2	0.81	0.92

[a] Calculated from Fig. 1b. [b] Adapted from Table 1.

of 2.0% LDS films for each method are listed in Table 4 and the average values ($\Delta J_{sc}\%_{avg}$) are also given.

It is shown in Table 4 that values of $\Delta J_{sc}\%$ obtained from these three methods are not exactly equal to each other. The differences in $\Delta J_{sc}\%$ are mainly caused by using different instruments and light sources in the measurements. The difference between $\Delta J_{sc}\%_{ph}$ obtained directly from photocurrent (I_{ph}) measurements and $\Delta J_{sc}\%_{I-V}$ obtained from short circuit current (I_{sc}) measured using a multimeter is caused by different external electrical loads applied in the measuring system. In addition, $\Delta J_{sc}\%_{EQE}$ values are lower than the others because the light from a solar simulator is not exactly the same as the AM1.5G solar spectrum. The xenon lamp in the solar simulator may have more short-wavelength light than that of the AM1.5G sunlight. In order to make meaningful comparisons between these fluorophores, average values of $\Delta J_{sc}\%$ were used and believed to be more reliable. The $\Delta J_{sc}\%_{avg}$ value of 2.0% LDS films containing fluorophores **1a–c** is 3.95%, 5.69% and 1.74%, respectively. Compared to Y083, fluorophores **1a** and **1b** exhibit stronger J_{sc} enhancing effects while fluorophore **1c** exhibits less effects. The differences in $\Delta J_{sc}\%_{avg}$ between these fluorophores can be explained by the three critical parameters listed in Table 4 – $J_{loss}\%$, F_{em} and $\Phi_{f,solid}$. As discussed before, $J_{loss}\%$ indicates the parasitic absorption effect of the fluorophore, and high $J_{loss}\%$ means the fluorophore exhibits red-shifted absorption and thus exhibits much spectral overlaps with the spectral response of the CdTe solar cell. F_{em} indicates the degree that emission spectrum matches with the spectral response of the CdTe solar cell, and high F_{em} means the fluorophore exhibits red-shifted emission. $\Phi_{f,solid}$ is the solid state fluorescence quantum yield of a fluorophore, indicating the photon conversion efficiency from photon absorption to photon emission. The calculated $J_{loss}\%$ and F_{em} values are consistent with the spectral shift observed in Fig. 1b as well as the photophysical parameters listed in Table 1. The order of absorption spectral shift of these fluorophores from red to blue is Y083 > **1b** > **1c** > **1a** (Table 1), which is consistent with the order of $J_{loss}\%$ in Table 4. The order of emission spectral shift of these fluorophores from red to blue is **1b** > Y083 > **1c** > **1a** (Table 1), which is also consistent with the order of F_{em} values in Table 4. From the analyses of the impacts of three parameters on $\Delta J_{sc}\%_{avg}$ in Table 4, it can be concluded that to achieve high $\Delta J_{sc}\%_{avg}$, the fluorophore should exhibit low $J_{loss}\%$ but high F_{em} and $\Phi_{f,solid}$, *i.e.* with blue-shifted absorption but red-shifted emission and near unity solid state fluorescence quantum yield. Among the three fluorophores, fluorophores **1a** and **1b** exhibit higher $\Delta J_{sc}\%_{avg}$ (3.95% and 5.69%, respectively) than that of Y083 (3.28%) because they have either a low $J_{loss}\%$ (4.0% for **1a**) or a high F_{em} (0.86 for **1b**). For fluorophore **1c**, the lower $\Delta J_{sc}\%_{avg}$ (1.74%) than that of Y083 (3.28%) is mainly caused by its low $\Phi_{f,solid}$ (0.81), which is at least over 10% lower than that of Y083 (0.92), fluorophores **1a** (0.99) and **1b** (0.98), suggesting more than 10% photon loss during the LDS process.

In order to further investigate the J_{sc} enhancement effects of these fluorophores, $\Delta J_{sc}\%_{ph}$ was recorded with the LDS films with various fluorophore concentrations of each fluorophore.

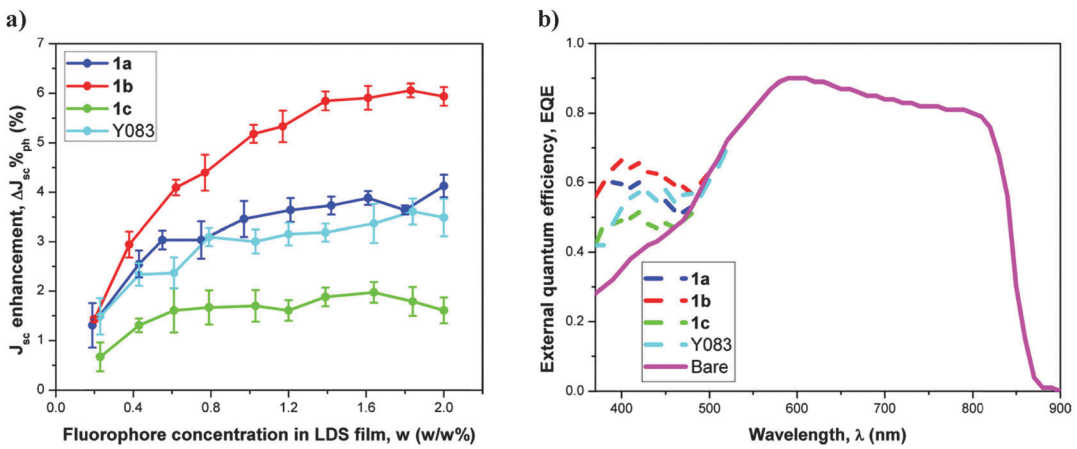

Fig. 4 (a) $\Delta J_{sc}\%_{ph}$ of the LDS films containing various concentrations of each fluorophore and (b) the spectral response (EQE) of a CdTe solar cell with a 2.0% LDS film of each fluorophore.

Moreover, the effect of a 2.0% LDS film of each fluorophore on the spectral response (EQE) of the CdTe solar cell was also studied. The experimental results are depicted in Fig. 4.

Fig. 4a shows, with the increase in the concentration of each fluorophore in the LDS film, $\Delta J_{sc}\%_{ph}$ gradually increases and reaches the plateau. The estimated concentration of $\Delta J_{sc}\%_{ph}$ to reach its plateau is 1.2% for each fluorophore. The observed increasing patterns of $\Delta J_{sc}\%_{ph}$ with the fluorophore concentrations in LDS film are governed by the Beer–Lambert law. An increase in the concentration of the fluorophore in LDS films within the lower concentration range can significantly affect the absorbance of the LDS film, *i.e.* the more fluorophores in the LDS film the more short-wavelength photons will be absorbed and converted into long-wavelength photons, therefore increase the $\Delta J_{sc}\%_{ph}$. However, since the concentration is an exponential function of absorbance, a further increase in the fluorophore concentration in the LDS films within the higher concentration range will attenuate the concentration effect on $\Delta J_{sc}\%_{ph}$ and ultimately lead to a maximum effect on $\Delta J_{sc}\%_{ph}$ (Fig. 4a). Also, a further increase in the concentration ($>4\%$) will block the incident light and affect the cell performance.[11] For fluorophores **1a–c** and Y083, this maximum is estimated to be 4.12%, 5.94%, 1.61% and 3.48% (Table 4), respectively. As the maximum effects on $\Delta J_{sc}\%_{ph}$ are achieved, it is expected that the spectral response of the CdTe solar cell to a short-wavelength will be significantly enhanced. The expected enhancements in the spectral response (EQE) to a short-wavelength for each fluorophore are shown in Fig. 4b. The EQE of a CdTe solar cell at 400 nm was enhanced from 0.35 to a magnitude between 0.49 and 0.67 by these fluorophores while EQE over 500 nm was not affected, showing the same response level with the bare cell. It is noted that these EQE enhancements in short-wavelength by LDS films are significant, compared to any other methods upon modifying the cell internal structure.[5–7]

The superior J_{sc} enhancement effects of fluorophores **1a** and **1b** over Y083, demonstrated by these small CdTe solar experiments, encouraged us to do further investigation on the effects on a large CdTe solar panel. 2.0% LDS film samples containing each fluorophore (**1a** and **1b**) as well as Y083 (Fig. 5a) were doped on the surface of a large CdTe solar panel. For the large CdTe solar panel, the measurements of its spectral response (EQE) and the *I–V* curve are impossible due to its bulk and heavy weight. Therefore, an alternative method was developed, in which the CdTe solar panel was placed directly in the sunlight and its output photocurrent ($I_{ph,panel}$) at various solar power densities (H) was recorded. The slopes of the obtained $I_{ph,panel}$ and H relationship were derived by linear fitting (Fig. 5b). Comparing the slope of the $I_{ph,panel}$ and H relationship of the bare panel to the slopes of the $I_{ph,panel}$ and H relationship of the panel with LDS films enables us to obtain the J_{sc} enhancement percentage ($\Delta J_{sc}\%_{ph,panel}$) of each fluorophore. The detailed data processing protocols are described in the Experimental section.

From Fig. 5a, it is obvious that all LDS films were uniformly doped on the CdTe solar panel surface without any air bubble between interfaces. The color of the LDS films containing fluorophores **1a**, **1b** and Y083 is green, deep green and dark yellow, respectively. For both bare and LDS film doped CdTe solar panels, their output photocurrent ($I_{ph,panel}$) exhibit good linear relationship with the incident solar power density (H). $\Delta J_{sc}\%_{ph,panel}$ of fluorophores **1a**, **1b** and Y083 calculated from linear fitting the results in Fig. 5b is 6.02%, 8.88% and 4.01%

Table 5 $\Delta J_{sc}\%_{ph,panel}$ calculated for fluorophores **1a**, **1b** and Y083, and its comparison with $\Delta J_{sc}\%_{ph}$ ($\Delta(\Delta J_{sc}\%_{ph})\% = \Delta J_{sc}\%_{ph,panel}/\Delta J_{sc}\%_{ph} - 1$)

Fluorophore	Slope ($\times 10^3$)	$\Delta J_{sc}\%_{ph,panel}$ (%)	$\Delta J_{sc}\%_{ph}$[a] (%)	$\Delta(\Delta J_{sc}\%_{ph})\%$ (%)
Bare	3.49 ± 0.004 (k_0)	0	0	0
1a	3.70 ± 0.003	6.02	4.12	46
1b	3.80 ± 0.004	8.88	5.94	49
Y083	3.63 ± 0.003	4.01	3.48	15

[a] Adapted from Table 4.

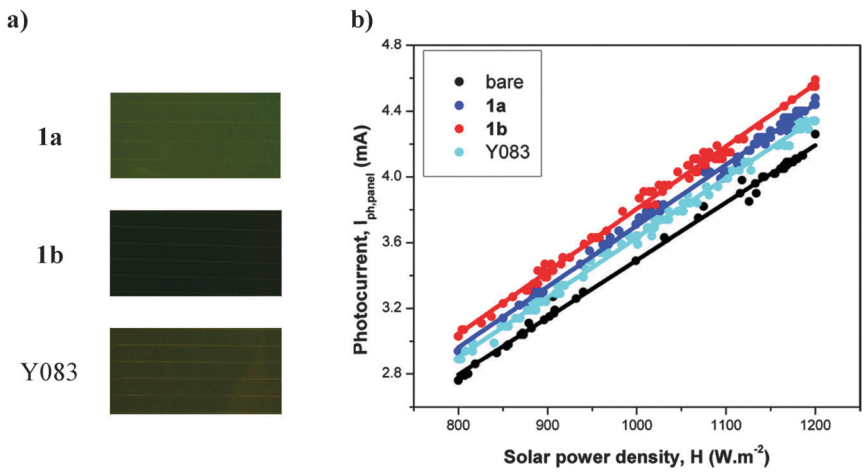

Fig. 5 (a) Surface images of a LDS film doped CdTe solar panel and (b) the linear relationship between photocurrent ($I_{ph,panel}$) and solar power density (H) of the bare solar panel and the LDS film doped solar panel.

(Table 5), respectively. In Table 5, $\Delta(\Delta J_{sc}\%_{ph})\%$ is defined as the percentage increase in $\Delta J_{sc}\%$ between the CdTe small cell and large panel experiments. The $\Delta(\Delta J_{sc}\%_{ph})\%$ values of these fluorophores are 46%, 49% and 15% higher than the $\Delta J_{sc}\%_{ph}$ value obtained from the small CdTe solar cell. Such an increase in $\Delta J_{sc}\%$ of the CdTe solar cell from a small unit to a large module can be attributed to the minimized photon side loss in the larger device because of the large surface area (225 cm^2) of the panel compared to the area (1 cm^2) of the small cell. Among the fluorophores tested with the large panel, Y083 only exhibits 15% increase in its $\Delta(\Delta J_{sc}\%_{ph})\%$ value, which is due to its weak photo-/thermo-stability under intensive sunlight during the long time course of the measurement.[30]

Conclusion

In conclusion, in this work, we proposed the rational design of a series of fluorophores as effective and efficient LDS molecules. In these fluorophores, the TPE group serves as a charge donor as well as an AIE functional group while the di-cyano group serves as a charge acceptor. All fluorophores possess the advantage of both molecular ICT and AIE mechanisms, exhibiting large Stokes shifts (up to 170 nm) and high solid state fluorescence quantum yields (up to 0.99). Their photophysical properties are highly related to their chemical structures. Compared to a traditional LDS molecule, Y083, they have less parasitic absorption effect ($J_{loss}\%$ as low as 4.0%) and/or higher degree of emission spectral matching (F_{em} up to 0.86) with the CdTe solar cell. Applying their solid PMMA films on a small CdTe solar cell and a large CdTe solar panel can enhance the output J_{sc} by as high as 5.69% and 8.88%, respectively, which are superior to Y083 (3.28% and 4.01%).

Experimental approaches

Synthetic procedures and compound characterization of fluorophores 1a–c

2-(4-(1,2,2-Triphenylvinyl)benzylidene)malononitrile (1a). *Reaction (ii)*: to a solution of compound **2** (1.2 g, 3.5 mmol) and malononitrile (343 mg, 5.2 mmol) in 50 mL of DCM was added Al_2O_3 (basic) (705 mg, 6.9 mmol). The reaction mixture was refluxed for 16 h. After 16 h, the reaction mixture was filtered. The solvent was removed and the residue was purified by silica gel chromatography using Hex/DCM (3 : 2) as an eluent to afford compound **1a** (isolated yield 75%). Yellow solid. ^{1}H-NMR (300 MHz, $CDCl_3$, δ): 7.67 (s, 1H), 7.63 (d, 2H, J = 5.9 Hz), 7.20–7.11 (m, 11H), 7.06–7.00 (m, 6H). ^{13}C-NMR (75 MHz, $CDCl_3$, δ): 159.4, 151.5, 144.3, 143.0, 143.0, 142.8, 139.5, 132.7, 131.6, 131.5, 130.6, 129.1, 128.3, 128.0, 127.7, 127.4, 127.3, 114.3, 113.1, 81.5. MALDI-MS: m/z calcd for $C_{27}H_{20}O^-$ 408.1626, found 408.1109.

2,3-Bis(4-(1,2,2-triphenylvinyl)phenyl)fumaronitrile (1b). *Reaction (v)*: a mixture of compound **4** (376 mg, 0.8 mmol), 2-bromo-1,1,2-triphenylethylene (784 mg, 2.3 mmol), $Pd(PPh_3)_4$ (90 mg, 10.0 mol%), K_2CO_3 (323 mg, 2.3 mmol, dissolved in 1 mL of water) and 1 mL of MeOH in 25 mL of toluene was stirred at 80 °C for 16 h. Then the reaction mixture was cooled down and extracted with DCM. The combined organic layer was dried over anhydrous $MgSO_4$ and filtered. The solvent was removed and the residue was purified by silica gel chromatography using Hex/DCM (2 : 1) as an eluent to afford compound **1b** (isolated yield 48%). Yellow solid. ^{1}H-NMR (300 MHz, $CDCl_3$, δ): 7.55 (d, 4H, J = 8.6 Hz), 7.18–7.10 (m, 22H), 7.07–7.00 (m, 12H). ^{13}C-NMR (75 MHz, $CDCl_3$, δ): 147.8, 143.4, 143.2, 143.2, 143.1, 139.7, 132.3, 131.6, 131.5, 131.5, 130.2, 128.2, 128.2, 128.2, 127.9, 127.3, 127.1, 124.4, 117.0. MALDI-MS: m/z calcd for $C_{56}H_{38}N_2^+$ 738.3035, found 738.4493.

2,2′-(4,4′-(1,2-Diphenylethene-1,2-di-yl)bis(4,1-phenylene))bis(methan-1-yl-1-ylidene)dimalononitrile (1c). *Reaction (viii)*: Al_2O_3 (575 mg, 5.6 mmol) was added to a solution of compound **6** (274 mg, 0.71 mmol) and malononitrile (186 mg, 2.8 mmol) in 50 mL of DCM. After reflux for 16 h, the reaction mixture was cooled to room temperature and filtered. The solvent was removed and the residue was purified by silica gel chromatography using Hex/EtOAc (5 : 1) as an eluent to afford compound **1c** (isolated yield 38%). Orange solid. ^{1}H-NMR (300 MHz, $CDCl_3$, δ): 7.72–7.64 (m, 6H), 7.21–7.15 (m, 10H), 7.02–6.97 (m, 4H). ^{13}C-NMR (75 MHz, $CDCl_3$, δ): 159.2, 159.1, 150.2, 150.1, 142.3, 142.2, 142.0, 141.8, 132.7, 132.6, 131.5, 131.4, 130.8, 130.6, 129.9, 129.6, 128.7, 128.4, 128.3, 128.0, 114.1, 114.1, 112.9, 82.5, 82.2. MALDI-MS: m/z calcd for $C_{34}H_{20}N_4^-$ 484.1688, found 484.1537.

Thermal stability measurements

Thermal stabilities were studied on Perkin-Elmer TGA 7 and DSC 7. TGA analysis was performed under ambient conditions from 30 °C to 450 °C at a rate of 10 °C min^{-1}. The typical mass used for DSC runs was 3.0–3.5 mg. The scans were performed from 50 °C to 325 °C at a rate of 10 °C min^{-1}. Decomposition temperature (T_d) is defined at the point of 5% mass loss.

Spectroscopic measurements

Absorption spectra were recorded using a Beckman Coulter DU730 Life Science UV-Vis spectrophotometer at room temperature. Emission spectra were collected on an ISS PC1 photon counting spectrofluorometer at room temperature. Fluorescence lifetimes were measured on a HORIBA JOBIN YVON fluorocube using 459 nm LED as the excitation light source with a 500 nm long pass filter at room temperature.

Theoretical calculations

Theoretical calculations were conducted using the Gaussian 09 package. All fluorophores were calculated in the gas phase without using the SCRF method to reduce the computational effort. Ground state (S_0) geometries were optimized by using the DFT B3LYP/6-31G(d) function. Excited state (S_1) geometries were optimized by using the time-dependent (TD) method with the same function. Single point calculations for the highest occupied molecular orbital (HOMO) and the lowest unoccupied molecular orbital (LUMO) were conducted at S_0 and S_1 optimal geometries.

LDS film preparation

Briefly, 7.5 g of PMMA powder (purchased from TCI America) was dissolved in 100 g of toluene in a 250 mL flask. The mixture was

stirred overnight and the insoluble PMMA was filtered off. Then, 2 g of the PMMA solution was finely mixed with variable amounts of each synthesized fluorophore in a 10 mL vial. The fluorophore–PMMA mixture was poured into a Petri dish ($R25 \times 15$ mm). The solvent was evaporated under ambient conditions and further dried in a vacuum oven at 60 °C for 1 h. The films were finally cut and peeled off from the Petri dish in warm water. The thickness of the prepared films is estimated to be about 50 μm.

Photovoltaic measurements

For the LDS measurements on the small CdTe solar cell (provided by Professor Alvin Compaan, University of Toledo),[31] a 150 W solar simulator (model# 96 000, Newport Corporation) equipped with a xenon lamp and an AM1.5G filter (model# 81 092, Newport Corporation) was used as the light source. The incident power density was 100 mW cm^{-2}, measured using a solar power meter (Amprobe SOLAR-100). Photocurrent (I_{ph}) was measured directly using a digital multimeter (GB electrical GDT200A). Short circuit current (I_{sc}) was obtained from the *I–V* curve measured using a sourcemeter (Keithley 2420 3A). EQE was measured from 370 to 800 nm in 10 nm steps on a modified fluorometer by using the same CdTe solar cell as the reference. Due to the small size of 1 cm^2 with the thickness of 3 mm of the cell, a large portion of photon loss (over 10%) from the side was expected during the measurements.[8] Index matching fluid was used to fill the interface between the LDS film and the front surface of the CdTe solar cell to reduce the refractive photon loss.

For the LDS studies on the large CdTe solar panel (First Solar FS-272), the LDS film was directly doped on the front surface (selected area of 225 cm^2) of the solar panel by the preparation method described previously but without the index matching fluid. For 2.0% LDS films, the amount of each fluorophore used for doping is 27 mg. The thickness of the LDS film was the same as the one studied on the small cell. The solar panel was set up in the campus (Washington State University, Pullman, United States) and mostly sunny with a little cloudy weather was chosen to achieve various power densities (H) of the incident sunlight ranging from 800 to 1200 W m^{-2} during the measurement. The measured photocurrent from the solar panel ($I_{ph,panel}$) shows a linear relationship with H for both the bare solar panel and the LDS film doped solar panel:

$$I_{ph,panel,0} = k_0 \times H \text{ (bare) and } I_{ph,panel,LDS} = k_{LDS} \times H \text{ (with LDS film)}$$

The J_{sc} enhancement effect of the fluorophore in the doped LDS film was calculated using:

$$\Delta J_{sc}\%_{ph,panel} = \frac{k_{LDS}}{k_0} - 1$$

Acknowledgements

We thank Professor Alvin Compaan (Department of Physics and Astronomy, The University of Toledo) for providing CdTe solar cells and Professor Kelvin G. Lynn (Center for Materials Research, Washington State University) for providing the instrument for *I–V* measurements.

References

1 M. Gloeckler, I. Sankin and Z. Zhao, *IEEE J. Photovoltaics*, 2013, **3**, 1389–1393.
2 P. Sinha, *Sol. Energy Mater. Sol. Cells*, 2013, **119**, 271–275.
3 M. A. Martinez, C. Guillen, M. T. Gutierrez and J. Herrero, *Sol. Energy Mater. Sol. Cells*, 1996, **43**, 297–310.
4 S. H. Demtsu and J. R. Sites, *31st IEEE Photovoltaic Specialists Conference*, 2005, pp. 347–350.
5 A. J. Clayton, S. J. C. Irvine, E. W. Jones, G. Kartopu, V. Barrioz and W. S. M. Brooks, *Sol. Energy Mater. Sol. Cells*, 2012, **101**, 68–72.
6 G. Gordillo, C. Calderon and H. Infante, *29th IEEE Photovoltaic Specialists Conference*, 2002, pp.644–647.
7 B. E. McCandless and S. S. Hecredus, *22nd IEEE Photovoltaic Specialists Conference*, 1991, pp. 967–972.
8 E. Klampaftis, D. Ross, K. R. McIntosh and B. S. Richards, *Sol. Energy Mater. Sol. Cells*, 2009, **93**, 1182–1194.
9 T. Maruyama and R. Kitamura, *Sol. Energy Mater. Sol. Cells*, 2001, **69**, 207–216.
10 L. Danos, T. Parel, T. Markvart, V. Barrioz, W. S. M. Brooks and S. J. C. Irvine, *Sol. Energy Mater. Sol. Cells*, 2012, **98**, 486–490.
11 B. S. Richards and K. R. McIntosh, *Prog. Photovoltaics*, 2007, **15**, 27–34.
12 D. Ross, E. Klampaftis, J. Fritsche, M. Bauer and B. S. Richards, *Sol. Energy Mater. Sol. Cells*, 2012, **103**, 11–16.
13 D. Ross, D. Alonso-Alvarez, E. Klampaftis, J. Fritsche, M. Bauer, M. G. Debije, R. M. Fifield and B. S. Richards, *IEEE J. Photovoltaics*, 2013, **4**, 457–646.
14 Y. Li, Z. Li, Y. Wang, A. Compaan, T. Ren and W.-J. Dong, *Energy Environ. Sci.*, 2013, **6**, 2907–2911.
15 F. B. Dias, S. Pollock, G. Hedley, L. O. Palsson, A. Monkman, I. I. Perepichka, II, I. F. Perepichka, M. Tavasli and M. R. Bryce, *J. Phys. Chem. B*, 2006, **110**, 19329–19339.
16 Z. R. Grabowski, K. Rotkiewicz and W. Rettig, *Chem. Rev.*, 2003, **103**, 3899–4032.
17 K. C. Moss, K. N. Bourdakos, V. Bhalla, K. T. Kamtekar, M. R. Bryce, M. A. Fox, H. L. Vaughan, F. B. Dias and A. P. Monkman, *J. Org. Chem.*, 2010, **75**, 6771–6781.
18 Y. L. Li, T. H. Ren and W. J. Dong, *J. Photochem. Photobiol., A*, 2013, **251**, 1–9.
19 Y. L. Li, L. Scudiero, T. H. Ren and W. J. Dong, *J. Photochem. Photobiol., A*, 2012, **231**, 51–59.
20 N. I. Nijegorodov and W. S. Downey, *J. Phys. Chem.*, 1994, **98**, 5639–5643.
21 I. B. Berlman, *J. Phys. Chem.*, 1970, **74**, 3085–3093.
22 W. Z. Yuan, P. Lu, S. M. Chen, J. W. Y. Lam, Z. M. Wang, Y. Liu, H. S. Kwok, Y. G. Ma and B. Z. Tang, *Adv. Mater.*, 2010, **22**, 2159–2163.
23 Z. J. Zhao, C. Y. K. Chan, S. M. Chen, C. M. Deng, J. W. Y. Lam, C. K. W. Jim, Y. N. Hong, P. Lu, Z. F. Chang,

X. P. Chen, P. Lu, H. S. Kwok, H. Y. Qiu and B. Z. Tang, *J. Mater. Chem.*, 2012, **22**, 4527–4534.
24 Y. Hong, J. W. Lam and B. Z. Tang, *Chem. Soc. Rev.*, 2011, **40**, 5361–5388.
25 K. Lee, J. Lee, E. J. Jeong, A. Kronk, K. S. Elenitoba-Johnson, M. S. Lim and J. Kim, *Adv. Mater.*, 2012, **24**, 2479–2484.
26 J. R. Lakowicz, *Principles of Fluorescence Spectroscopy*, Springer Science + Business Media, LLC, NY, USA, 3rd edn, 2006.
27 E. Lippert, *Z. Naturforsch., A: Phys. Sci.*, 1955, **10**, 541–545.
28 N. Mataga, Y. Kaifu and M. Koizumi, *Bull. Chem. Soc. Jpn.*, 1955, **28**, 690–691.
29 N. Mataga, Y. Kaifu and M. Koizumi, *Bull. Chem. Soc. Jpn.*, 1956, **29**, 465–470.
30 Z. Jiang, R. Bogumila, H. Zhang, P. Wang, M. Yamamoto and S. Wang, US 2013/0284265 A1, 2013.
31 A. Gupta and A. D. Compaan, *Appl. Phys. Lett.*, 2004, **85**, 684–686.